Galactic orbital motions in the dark matter, modified Newtonian dynamics and modified gravity scenarios

L. Iorio[★]

INFN-Sezione di Pisa, Viale Unità di Italia 68, 70125, Bari (BA), Italy

ABSTRACT

We simultaneously integrate in a numerical way the equations of motion of both the Magellanic Clouds (MCs) in the MOdified Newtonian Dynamics (MOND), MOdified Gravity (MOG) and cold dark matter (CDM) frameworks for $-1 \leq t \leq 1$ Gyr in order to see if, at least in principle, it is possible to discriminate between them. Since the Large Magellanic Cloud (LMC) and the Small Magellanic Cloud (SMC) are at distances of approximately 50–60 kpc from the centre of the Milky Way (MW), they are ideal candidates for investigating the deep MOND regime occurring when the characteristic MOND acceleration $A_0 = 1.2 \times 10^{-10}$ m s^{-2} is larger than the internal acceleration A of the system considered; indeed, the Newtonian baryonic accelerations A_N involved are about 0.02–0.03A_0 for them. It turns out that CDM, MOND and MOG yield, in fact, different trajectories. In MOND the external field effect A_{ext} must, in principle, also be considered. Since for the MW $A_{ext} \approx 0.01A_0$, with a lingering uncertainty, we consider both the cases $A_{ext} < A_N$, $A_{ext} \ll A_0$ and $A_{ext} = A_N$, $A_{ext} \ll A_0$. We also investigate the impact of the current uncertainties in the velocity components of MCs on their motions in the theories considered. In modelling the mutual interaction between the clouds and the dynamical friction (in CDM and MOND) we use for the masses of MCs the total (baryonic + dark matter) values, dynamically inferred, in CDM, and the smaller ones (baryonic), coming from direct detection of visible stars and neutral gas, in MOND and MOG.

Key words: gravitation – methods: numerical – Galaxy: general – galaxies: kinematics and dynamics – Magellanic Clouds – dark matter.

1 INTRODUCTION

In many astrophysical systems, such as spiral galaxies and clusters of galaxies, a discrepancy between the observed kinematics of some of their components and the predicted one on the basis of the Newtonian dynamics and the matter directly detected from the emitted electromagnetic radiation (visible stars and gas clouds) was present since the pioneering studies by Zwicky (1933)[1] on the Coma cluster and by Bosma (1981) and Rubin et al. (1982) on spiral galaxies. More precisely, such an effect shows up in the galactic velocity rotation curves (Persic, Salucci & Stel 1996a,b) whose typical pattern after a few kiloparsecs from the centre differs from the Keplerian $1/\sqrt{r}$ fall-off expected from the usual Newtonian dynamics applied to the electromagnetically observed matter.

As a possible solution to this puzzle, the existence of nonbaryonic, weakly interacting cold dark matter (CDM; in the sense

that its existence is indirectly inferred only from its gravitational action, not from emitted electromagnetic radiation) was proposed to reconcile the predictions with the observations (Rubin 1983) in the framework of the standard gravitational physics; for a general review on the CDM issue, see for example Khalil & Muñoz (2002), while for the distribution of CDM in galaxies, see for example Salucci & Borriello (2003). To be more definite, let us focus on the Milky Way (MW) and adopt a very widely used model of its gravitational potential U. It consists of the standard Miyamaoto–Nagai disc (Miyamoto & Nagai 1975):

$$U_{disc} = -\frac{\xi G M_{disc}}{\sqrt{x^2 + y^2 + \left(k + \sqrt{z^2 + b^2}\right)^2}}, \qquad (1)$$

the Plummer (1911) bulge:

$$U_{bulge} = -\frac{G M_{bulge}}{r + c} \qquad (2)$$

and the logarithmic CDM halo by Binney & Tremaine (1987):

$$U_{halo} = v_{halo}^2 \ln(r^2 + d^2) \quad \text{(spherical halo)} \qquad (3)$$

with (Law, Johnston & Majewski 2005; Willett et al. 2009) $\xi = 1, k = 6.5$ kpc, b = 0.26 kpc, c = 0.7 kpc, $v_{halo} = 114$ km s^{-1} and

[★]E-mail: lorenzo.iorio@libero.it

[1] He postulated the existence of undetected, baryonic matter; today, it is believed that the hidden mass is constituted by non-baryonic, weakly interacting particles in order to cope with certain issues pertaining galaxy formation and primordial nucleosynthesis (Gondolo 2004).

$d = 12$ kpc. The masses of the disc and the bulge used by Law et al. (2005) are those by Johnston et al. (1999), i.e. $M_{\mathrm{disc}} = 1 \times 10^{11}$ M$_\odot$ and $M_{\mathrm{bulge}} = 3.4 \times 10^{10}$ M$_\odot$ yielding a total baryonic mass of $M = 1.34 \times 10^{11}$ M$_\odot$; however, such a value is almost twice the most recent estimate ($M = 6.5 \times 10^{10}$ M$_\odot$) by McGaugh (2008) who includes the gas mass as well and yields $M_{\mathrm{disc}} = 2.89 \times 10^{10}$ M$_\odot$ and $M_{\mathrm{bulge}} = 2.07 \times 10^{10}$ M$_\odot$. Xue et al. (2008) yield a total baryonic mass of $M = 6.5 \times 10^{10}$ M$_\odot$ as well; they use a different bulge+disc+CDM halo model of the Galaxy with $M_{\mathrm{disc}} = 5 \times 10^{10}$ M$_\odot$ and $M_{\mathrm{bulge}} = 1.5 \times 10^{10}$ M$_\odot$, as in Smith et al. (2007). The model of equations (1)–(3), with the parameter values by Law et al. (2005) and Johnston et al. (1999), has been recently used by Willett et al. (2009) to study the motion of the Grillmair & Dionatos (2006) tidal stellar stream at a Galactocentric distance of $r \lesssim 16$–18 kpc; Read & Moore (2005) used it to study the motion of the tidal debris of the Sagittarius dwarf at 17.4 kpc from the centre of the MW. More specifically, the CDM halo model of equation (3) corresponds to a CDM halo mass:

$$M_{\mathrm{halo}} = \frac{2v_{\mathrm{halo}}^2 r^3}{G(r^2 + d^2)},\qquad(4)$$

so that

$$M_{\mathrm{halo}}(r = 60\,\mathrm{kpc}) = 3.5 \times 10^{11}\,\mathrm{M}_\odot,\qquad(5)$$

in agreement with the value by Xue et al. (2008):

$$M_{\mathrm{halo}}(r = 60\,\mathrm{kpc}) = (4.0 \pm 0.7) \times 10^{11}\,\mathrm{M}_\odot.\qquad(6)$$

Concerning v_{halo}, other authors report different values for it; for example Read & Moore (2005) use $v_0 = 175$ km s^{-1}, where $v_0^2 = 2v_{\mathrm{halo}}^2$, so that $v_{\mathrm{halo}} = 124$ km s^{-1} for them, while Johnston et al. (1999) yield the range 140–200 km s^{-1} for their $v_{\mathrm{circ}} = \sqrt{2}v_{\mathrm{halo}}$ which maps into 70 km s$^{-1} \leq v_{\mathrm{halo}} \leq 141$ km s^{-1}. However, it must be noted that values of v_{halo} too different from 114 km s^{-1} would destroy the agreement of equation (4) with the value of equation (6).

Oppositely, it was postulated that the Newtonian laws of gravitation have to be modified on certain acceleration scales to correctly account for the observed anomalous kinematics of such astrophysical systems without resorting to still undetected exotic forms of matter. One of the most phenomenologically successful modifications of the inverse-square Newtonian acceleration A_{N}, mainly with respect to spiral galaxies, is the MOdified Newtonian Dynamics (MOND; Milgrom 1983a,b,c) which postulates that for systems experiencing total gravitational acceleration $A \ll A_0$, with (Begeman, Broeils & Sanders 1991)

$$A_0 = (1.2 \pm 0.27) \times 10^{-10}\,\mathrm{m\,s^{-2}},\qquad(7)$$

$$\boldsymbol{A} \to \boldsymbol{A}_{\mathrm{MOND}} = -\frac{\sqrt{A_0 G M}}{r}\hat{\boldsymbol{r}}.\qquad(8)$$

More precisely, it holds

$$A = \frac{A_{\mathrm{N}}}{\mu(X)},\qquad X \equiv \frac{A}{A_0};\qquad(9)$$

$\mu(X) \to 1$ for $X \gg 1$, i.e. for large accelerations (with respect to A_0), while $\mu(X) \to X$ yielding equation (8) for $X \ll 1$, i.e. for small accelerations (again, with respect to A_0). The most widely used forms for the interpolating function $\mu(X)$ are the 'standard' (Bekenstein & Milgrom 1984)

$$\mu(X) = \frac{X}{\sqrt{1 + X^2}}\qquad(10)$$

and the simpler (Famaey & Binney 2005)

$$\mu(X) = \frac{X}{1 + X}.\qquad(11)$$

It recently turned out that equation (11) yields better results in fitting the terminal velocity curve of the MW, the rotation curve of the standard external galaxy NGC 3198 (Famaey & Binney 2005; Zhao & Famaey 2006; Famaey, Gentile & Bruneton 2007b) and the rotation curve of a sample of 17 high surface brightness, early-type disc galaxies (Sanders & Noordermeer 2007); equation (9) becomes

$$A = \frac{A_{\mathrm{N}}}{2}\left(1 + \sqrt{1 + \frac{4A_0}{A_{\mathrm{N}}}}\right)\qquad(12)$$

with equation (11). Equation (9) strictly holds for co-planar, spherically and axially symmetric mass distributions (Brada & Milgrom 1995); otherwise, the fully modified (non-relativistic) Poisson equation (Bekenstein & Milgrom 1984)

$$\nabla \cdot \left[\mu\left(\frac{|\nabla U|}{A_0}\right)\nabla U\right] = 4\pi G\rho\qquad(13)$$

must be used. Attempts to yield a physical foundation of MOND, especially in terms of a relativistic covariant theory, can be be found in, for example, Bekenstein & Milgrom (1984), Bekenstein (2004), Bruneton & Esposito-Farèse (2007) and Zhao (2007); for recent reviews of various aspects of the MOND paradigm, see Sanders & McGaugh (2002), Bekenstein (2006) and Milgrom (2008). The compatibility of MOND with Solar system data has been investigated by Milgrom (1983a), Talmadge et al. (1988), Sereno & Jetzer (2006), Bekenstein & Magueijo (2006), Sanders (2006), Iorio (2008a), Iorio (2009) and Milgrom (2009). Generally speaking, many theoretical frameworks have been set up to yield a $1/r$ acceleration term able to explain the observed dynamics of astrophysical systems; for example, those encompassing a logarithmic extra potential (Cadoni 2004; Fabris & Pereira Campos 2009)

$$U = C\ln\left(\frac{r}{r_{\mathrm{s}}}\right),\qquad(14)$$

where C and r_{s}, a length-scale, are fit-for parameters. For other modified models of gravity used to explain, among other things, the galactic rotation curves without resorting to CDM, see for example Capozziello et al. (2006), Frigerio-Martins & Salucci (2007) and Moffat & Toth (2008).

The MOdified Gravity (MOG; Moffat & Toth 2008) is a fully covariant theory of gravity which is based on the existence of a massive vector field coupled universally to matter. The theory yields a Yukawa-like modification of gravity with three constants which, in the most general case, are running; they are present in the theory's action as scalar fields which represent the gravitational constant, the vector field coupling constant and the vector field mass. An approximate solution to the MOG field equations (Moffat & Toth 2009) allows us to compute their values as functions of the source's mass. The resulting Yukawa-type modification of the inverse-square Newton's law in the gravitational field of a central mass M is

$$\boldsymbol{A}_{\mathrm{MOG}} = -\frac{G_{\mathrm{N}}M}{r^2}\left\{1 + \alpha\left[1 - (1 + \mu r)\exp(-\mu r)\right]\right\}\hat{\boldsymbol{r}},\qquad(15)$$

with[2]

$$\alpha \simeq \frac{M}{\left(\sqrt{M} + E\right)^2}\left(\frac{G_\infty}{G_{\mathrm{N}}} - 1\right),\qquad(16)$$

$$\mu \simeq \frac{D}{\sqrt{M}},\qquad(17)$$

---

[2] Moffat & Toth (2008) used the equivalent notation $E \to C_1'$ and $D \to C_2'$.

where G_N is the Newtonian gravitational constant and

$$G_\infty \simeq 20 G_N, \tag{18}$$

$$E \simeq 25\,000 \sqrt{M_\odot}, \tag{19}$$

$$D \simeq 6250 \sqrt{M_\odot} \; \text{kpc}^{-1}. \tag{20}$$

Such values have been obtained by Moffat & Toth (2008, 2009) as a result of the fit of the velocity rotation curves of some galaxies in the framework of the searches for an explanation of the rotation curves of galaxies without resorting to CDM. The validity of equation (15) in the Solar system has been recently questioned in Iorio (2008b). For (McGaugh 2008) $M = 6.5 \times 10^{10} \, M_\odot$, we have

$$\alpha \simeq 16 \tag{21}$$

$$\lambda = \frac{1}{\mu} \simeq 41 \, \text{kpc}. \tag{22}$$

Traditionally, the phenomenology of both MOND and CDM paradigms is based on the electromagnetically detected matter (stars and gas clouds) at no more than about 20 kpc; in view of the use by Clewley et al. (2004) and Xue et al. (2008) of several recently discovered blue horizontal-branch (BHB) stars as kinematical tracers at large radii ($r \approx 60$–130 kpc), it now makes sense to look at the remote periphery of the Galaxy as well to try to test CDM and alternative models of gravity. In this paper, we wish to investigate the orbits of test particles at Galactocentric distances $r > 20$ kpc, i.e. in the deep MONDian regime; we will use the Magellanic Clouds (MCs) moving at 50–60 kpc from the centre of the MW. We will also extend our analysis to MOG and to the action of CDM itself as well to see if our approach is able, at least in principle, to discriminate between them; for another attempt on galactic scales, based on the escape speed in the solar neighbourhood, see also Famaey, Bruneton & Zhao (2007a). At so large Galactocentric distances many complications arising from an accurate modelling of the realistic distribution of mass can be avoided, both in MOND/MOG and in CDM frameworks. Moreover, Gardiner & Noguchi (1996), Yoshizawa & Noguchi (2003) and Connors, Kawata & Gibson (2006) demonstrated that the position of the Magellanic Stream (MS) follows the orbits of MCs. Therefore, it is interesting to compare the path of MS with the orbits predicted by CDM, MOND and MOG. Thus, it is hoped that our results will encourage more quantitative and detailed studies on MOND and MOG applied to such systems; for numerical investigations on the problem of the formation of cosmological structures and galactic evolution, see Knebe & Gibson (2004), Haghi, Rahvar & Hasani-Zonooz (2006), Llinares, Knebe & Zhao (2008), Tiret & Combes (2007), Tiret & Combes (2008) and Malekjani, Rahvar & Haghi (2009).

2 MOTIONS IN CDM, MOND AND MOG: THE MAGELLANIC CLOUDS

Concerning MOND and MOG, we will consider a central body with the same mass (McGaugh 2008) $M \approx 6.5 \times 10^{10} \, M_\odot$ of the total baryonic component of the MW and a test particle distant several tens of kiloparsecs from it, acted upon by the putative MOND/MOG gravitational fields of M. Such large distances allow us to neglect the details of the real mass distribution which may become relevant in MOND at closer distances (Read & Moore 2005; Nipoti et al. 2007). To preliminarily test our approximation, we applied equation (12) to the Sagittarius dwarf galaxy ($r = 17.4$ kpc) and confronted the numerically integrated orbital sections in the coordinate planes of

the trajectory to those obtained by Read & Moore (2005) by using a non-pointlike baryonic potential (upper panel of fig. 2 in Read & Moore 2005); we used the same integration interval of $-1 \leq t \leq 1$ Gyr and the same baryonic mass ($M = 1.2 \times 10^{11} \, M_\odot$) by Read & Moore (2005). It turns out that we were successful in reproducing the orbital sections by Read & Moore (2005); thus, we are confident of the validity of our approximation for the larger Galactocentric distances we will use in the following analysis.

Another issue which, in principle, should be taken into account in MOND is the so-called external field effect (EFE); it may become relevant with a cluster of galaxies (Wu et al. 2007). According to, for example, Sanders & McGaugh (2002), Famaey et al. (2007a) and Angus & McGaugh (2008),

$$\mu \left(\frac{|A_{\text{ext}} + A|}{A_0} \right) A = A_N, \tag{23}$$

where A_N is the Newtonian acceleration of the system alone, A is its total internal acceleration while A_{ext} denotes the acceleration induced by any external field. By using the simpler form of equation (11) for μ, one approximately obtains from equation (23)

$$A \approx \frac{A_N}{2} \left[1 - \frac{A_{\text{ext}}}{A_N} + \sqrt{\left(1 - \frac{A_{\text{ext}}}{A_N} \right)^2 + \frac{4 A_0}{A_N} \left(1 + \frac{A_{\text{ext}}}{A_0} \right)} \right]. \tag{24}$$

For $A_0 \to 0$, $A \to A_N$, as expected. For $A_{\text{ext}} \to 0$, i.e. $A_{\text{ext}} \ll A_0$ and $A_{\text{ext}} \ll A_N$, one has $A \to$ equation (12). For

$$\frac{A_{\text{ext}}}{A_0} \ll 1 \tag{25}$$

only, the total acceleration becomes

$$A \approx \frac{A_N}{2} \left[1 - \frac{A_{\text{ext}}}{A_N} + \sqrt{\left(1 - \frac{A_{\text{ext}}}{A_N} \right)^2 + \frac{4 A_0}{A_N}} \right], \tag{26}$$

while for

$$\frac{A_{\text{ext}}}{A_N} \approx 1 \tag{27}$$

only, it is

$$A \approx \sqrt{A_N A_0 \left(1 + \frac{A_{\text{ext}}}{A_0} \right)}. \tag{28}$$

Interestingly, if

$$\frac{A_{\text{ext}}}{A_N} \approx 1, \quad \frac{A_{\text{ext}}}{A_0} \ll 1, \tag{29}$$

then

$$A \approx \sqrt{A_N A_0} = \frac{\sqrt{G M A_0}}{r}. \tag{30}$$

In the case of MW, it is very difficult to reliably assess the external field because it may be due to several factors such as the large-scale structure and the great attractor region ($A_{\text{ext}}/A_0 = 0.01$); galaxy M31 Andromeda, at 800 kpc from the MW, and the Coma and Virgo clusters, whose fields are time-varying, may also play a role. For a discussion, see Wu et al. (2008). In view of the lingering uncertainty of A_{ext}, in the following we will use equation (12); however, we will also investigate the case in which $A_{\text{ext}} = A_N$, $A_{\text{ext}} \ll A_0$ because it may occur in the MW at the large Galactocentric distances considered here.

As a concrete example of motion in the deep MOND regime ($A_N/A_0 \approx 0.03-0.02$), let us consider both MCs; the Large Magellanic Cloud (LMC) is at 49.4 kpc from the centre of the MW

Table 1. LMC: coordinates (Kallivayalil et al. 2006; Wu et al. 2008), in kpc, and velocity components (Wu et al. 2008), in km s^{-1}, of the LMC in a Galactocentric rest frame $\{X, Y, Z\}$ with the Z-axis pointing towards the Galactic North Pole, the X-axis pointing in the direction from the Sun to the GC and the Y-axis pointing in the direction of the Sun's Galactic rotation (Kallivayalil et al. 2006; Besla et al. 2007). They yield $r = 49.5$ kpc, $v = 378$ km s^{-1}. The uncertainties in the coordinates can be neglected (Cioni et al. 2000).

$X_0 = -0.8$	$Y_0 = -41.5$	$Z_0 = -26.9$
$\dot{X}_0 = -86 \pm 12$	$\dot{Y}_0 = -268 \pm 11$	$\dot{Z}_0 = 252 \pm 16$

Table 2. SMC: coordinates (Kallivayalil et al. 2006; Wu et al. 2008), in kpc, and velocity components (Wu et al. 2008), in km s^{-1}, of the SMC in a Galactocentric rest frame $\{X, Y, Z\}$ with the Z-axis pointing towards the Galactic North Pole, the X-axis pointing in the direction from the Sun to the GC and the Y-axis pointing in the direction of the Sun's Galactic rotation (Kallivayalil et al. 2006; Besla et al. 2007). They yield $r = 58.9$ kpc, $v = 301$ km s^{-1}. The uncertainties in the coordinates are negligible (Cioni et al. 2000).

$X_0 = 15.3$	$Y_0 = -36.9$	$Z_0 = -43.3$
$\dot{X}_0 = -87 \pm 48$	$\dot{Y}_0 = -247 \pm 42$	$\dot{Z}_0 = 149 \pm 37$

[Galactic Centre (GC)], while the Small Magellanic Cloud (SMC) is located at 59 kpc from the GC. LMC and SMC's Galactocentric Cartesian coordinates and velocities (Kallivayalil, van der Marel & Alcock 2006; Wu et al. 2008) are given in Tables 1 and 2. It can be noted that the velocity components of the LMC are uncertain at more than 4–14 per cent. The situation for the position components is much better since they are known with uncertainties in the range of 0.1–1 per cent, as it results from the analysis of the tip of the red giant branch (TRGB) applied to MCs by Cioni et al. (2000); thus, we will neglect them in the following. Also for SMC the uncertainty in the position components is negligible (Cioni et al. 2000), while the velocity components are known at 10 per cent.

We simultaneously integrated in a numerical way the equations of motion of both MCs in MOND, MOG and CDM by using the initial conditions of Tables 1 and 2 for $-1 \leq t \leq 1$ Gyr. In addition to the main pull due to the MW, we also included the mutual attractions of MCs and the effect of the dynamical friction due to their motion through the Galactic dark halo (Binney & Tremaine 1987); the mutual dynamical friction was neglected (Kallivayalil et al. 2006). Concerning the pull by the LMC on the SMC, we modelled its action in Newtonian dynamics from a Plummer (1911)-type potential (Kallivayalil et al. 2006):

$$U_{\rm LMC} = \frac{Gm_{\rm LMC}}{\sqrt{(x - x_{\rm LMC})^2 + (y - y_{\rm LMC})^2 + (z - z_{\rm LMC})^2 + K_{\rm LMC}^2}},$$
(31)

with $K_{\rm LMC} = 3$ kpc. In MOND, since the acceleration imparted by the LMC on the SMC is of the order of about $0.05A_0$, we adopted equation (8) with $M \rightarrow m_{\rm LMC}$ and $r = \sqrt{(x - x_{\rm LMC})^2 + (y - y_{\rm LMC})^2 + (z - z_{\rm LMC})^2 + K_{\rm LMC}^2}$, while in MOG we used equation (15) with $M \rightarrow m_{\rm LMC}$ and $r = \sqrt{(x - x_{\rm LMC})^2 + (y - y_{\rm LMC})^2 + (z - z_{\rm LMC})^2 + K_{\rm LMC}^2}$. An analogous expression for the pull by the SMC on the LMC holds; in this case, $K_{\rm SMC} = 2$ kpc (Kallivayalil et al. 2006). The dynamical friction experienced by, say, the SMC in going through the dark

halo of the Galaxy has been modelled, in CDM, as

$$\boldsymbol{D} = -\frac{\boldsymbol{v}}{t_{\rm fric}},$$
(32)

with (Kallivayalil et al. 2006; Haghi, Hasani-Zonooz & Rahvar 2009)

$$t_{\rm fric}^{-1} \approx 0.428 \ln \Lambda \frac{Gm_{\rm SMC}}{r^2 v},$$
(33)

where the Coulomb logarithm $\ln \Lambda \approx 3$ (Binney & Tremaine 1987). We also included the mutual dynamical friction experienced by the SMC when its distance from the LMC gets smaller than 15 kpc (Bekki & Chiba 2005; Kallivayalil et al. 2006) by replacing in equation (33) $\ln \Lambda = 3$ with $\ln \Lambda_{\rm LS} = 0.2$ and r with $r_{\rm mutual}$. The dynamical friction also plays a non-negligible role in several astrophysical systems in the framework of MOND (Ciotti & Binney 2004; Sánchez-Salcedo, Reyes-Iturbide & Hernandez 2006; Nipoti et al. 2008); in our case, we model it by assuming (Ciotti & Binney 2004; Nipoti et al. 2008)

$$\frac{t_{\rm fric}^{\rm MOND}}{t_{\rm fric}^{\rm N}} = \frac{\sqrt{2}}{1 + \frac{A}{A_{\rm N}}} \approx \frac{\sqrt{2}}{1 + \sqrt{\frac{A_0}{GM}r}}.$$
(34)

Since a model of the dynamical friction has not yet been developed in the framework of MOG, we did not include it.

Concerning the masses of MCs entering both their mutual interactions and the dynamical friction, for consistency reasons we adopted the total (baryonic + dark matter) values $m_{\rm LMC} = 2 \times 10^{10}$ M$_\odot$ (Schommer et al. 1992; Gardiner & Noguchi 1996; Kallivayalil et al. 2006; Haghi et al. 2009), coming from radial velocities of several of the oldest star clusters in the LMC lying well beyond 6 kpc from its centre, and[3] $m_{\rm SMC} = 3 \times 10^9$ M$_\odot$ (Kallivayalil et al. 2006; Haghi et al. 2009) when integrating the CDM model. Instead, we used the smaller, baryonic values $m_{\rm LMC} = (2.7 + 0.5 = 3.2) \times 10^9$ M$_\odot$ (visible disc + neutral gas; Kim et al. 1998) (van der Marel et al. 2002; van der Marel, Kallivayalil & Besla 2009) and $m_{\rm SMC} = (3.1 + 5.6 = 8.7) \times 10^8$ M$_\odot$ (total stellar mass + neutral gas) (van der Marel et al. 2009) for MOND and MOG, respectively. For a recent discussion of the methods employed to obtain such figures and of other results, see van der Marel et al. 2009.

2.1 The Large Magellanic Cloud

In Fig. 1, we show the sections in the coordinate planes of the LMC's orbits for CDM (red dash–dotted curves), MOND (blue dashed lines and light blue dotted lines) and MOG (yellow continuous curves) over $-1 \leq t \leq 1$ Gyr. The dynamical models and their parameter values are those described in Section 2. We used equation (12) for MOND ($A_{\rm ext} \ll A_{\rm N}$ and $A_{\rm ext} \ll A_0$) obtaining the blue dashed lines depicted; indeed, for LMC $A_{\rm N}/A_0 = 0.03$, so that equation (12) is adequate for it by assuming $A_{\rm ext} = 0.01A_0$. Concerning the impact of EFE in MOND on the LMC, we also investigated it in the case $A_{\rm ext} = A_{\rm N}$ and $A_{\rm ext} \ll A_0$; thus, we numerically integrated trajectories with equation (30) as well, which corresponds to an external field equal to the internal Newtonian one, obtaining the light blue dotted curves shown. The same approach will be used in Section 2.2 for the SMC. The middle panel of Fig. 2 shows the Galactocentric distance of the

---

[3] This typical value has been chosen by Kallivayalil et al. (2006) after an examination of the values coming from observations of carbon stars (Hardy, Suntzeff & Azzopardi 1989) and planetary nebulæ (Dopita et al. 1985), and from a virial analysis of the kinematics of thousands of red giant stars in SMC (Harris & Zaritsky 2006).
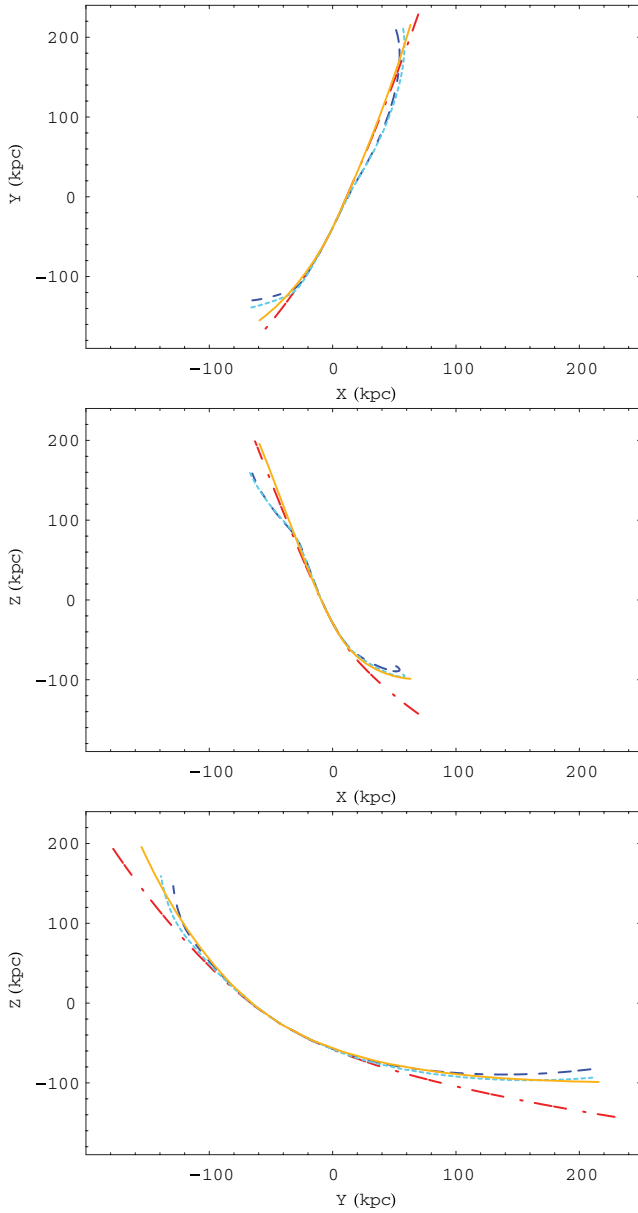
Figure 1. Sections in the coordinate planes of the numerically integrated trajectories of LMC experiencing (a) the Newtonian acceleration with CDM (red dash–dotted line), (b) the MOND acceleration with $\mu = X/(1 + X)$ (blue dashed line), (c) the MOND acceleration with $\mu = X$ (light blue dotted line) and (d) the MOG acceleration (yellow continuous line). The central values of the initial conditions of Table 1 have been used. For the baryonic masses of the MW's bulge and disc, we used the values by McGaugh (2008), with a total baryonic mass of $M = 6.5 \times 10^{10}\,M_\odot$. For the masses of MCs, entering their mutual interactions and the dynamical friction, both modelled in the present integration, the total values (baryonic + dark matter) have been adopted for CDM, while those encompassing only baryonic components have been used for MOG and MOND. The time-span of the integration is $-1 \leq t \leq 1$ Gyr.

LMC for the central values of the velocity components of Table 1 over $-1 \leq t \leq 1$ Gyr.

The smallest Galactocentric distance occurs for MOND, while MOG and CDM yield the largest one amounting to about 255–270 kpc after $+1$ Gyr and 250–280 kpc after -1 Gyr. MOG and CDM differ by about 15 kpc, while the discrepancy between MOG/CDM and MOND is approximately 70–80 kpc after -1 Gyr;
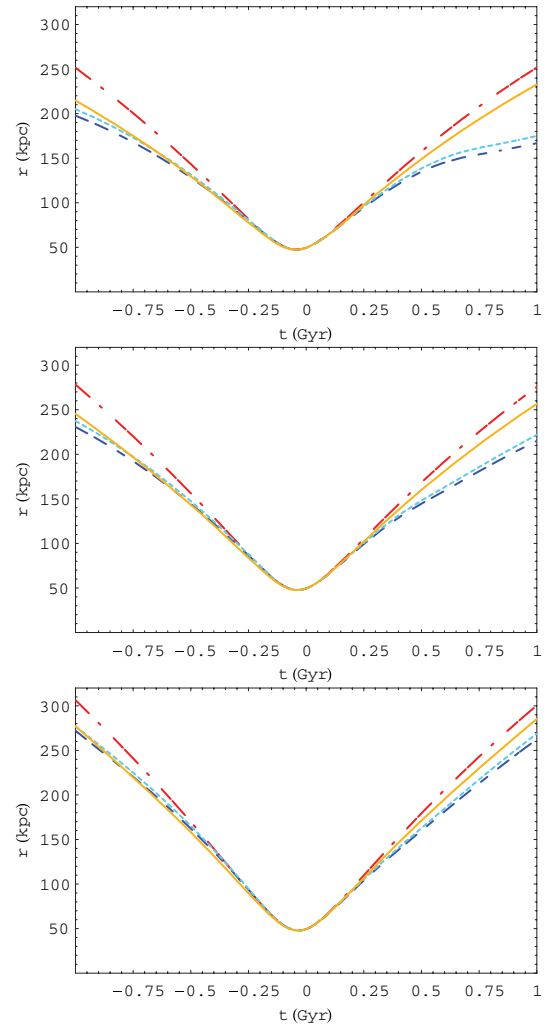
Figure 2. LMC: galactocentric distance r, in kpc, for $-1 \leq t \leq 1$ Gyr. Red dash–dotted line: CDM. Blue dashed line: MOND ($\mu = X/(1 + X)$). Light blue dotted line: MOND ($\mu = X$). Yellow continuous line: MOG. The initial condition for the position is $r = 49.4$ kpc. Upper panel: for the velocity we adopted $\dot{x}_0 = -86 + 12 = -74\,\mathrm{km\,s^{-1}}$, $\dot{y}_0 = -268 + 11 = -257\,\mathrm{km\,s^{-1}}$, $\dot{z}_0 = 252 - 16 = 236\,\mathrm{km\,s^{-1}}$ yielding the minimum value $v = 356.7\,\mathrm{km\,s^{-1}}$. Middle panel: the central values of Table 1 have been adopted for the velocity. Lower panel: for the velocity we adopted $\dot{x}_0 = -86 - 12 = -98\,\mathrm{km\,s^{-1}}$, $\dot{y}_0 = -268 - 11 = -279\,\mathrm{km\,s^{-1}}$, $\dot{z}_0 = 252 + 16 = 268\,\mathrm{km\,s^{-1}}$ yielding the maximum value $v = 399.1\,\mathrm{km\,s^{-1}}$. For the masses of MCs, entering their mutual interactions and the dynamical friction, both modelled in this integration, the total values (baryonic + dark matter) have been adopted for CDM, while those encompassing only baryonic components have been used for MOG and MOND.

in the past Gyr, the discrepancy between MOG and CDM is of the order of 30 kpc, while MOND differs from MOG/CDM by a few 10 kpc. Over the next Gyr, the Galactocentric distance of the LMC undergoes a steady increase. It maybe interesting to recall that, according to Wu et al. (2008), the LMC is on a bound orbit; however, they did not include either the mutual interaction with the SMC or the dynamical friction. The difference between the MOND trajectories for $\mu = X/(1 + X)$ and $\mu = X$ is rather small; discrepancies of the order of 10 kpc or less occur at ± 1 Gyr. All the models considered tend to undergo reciprocal departures after some about ± 500 Myr.
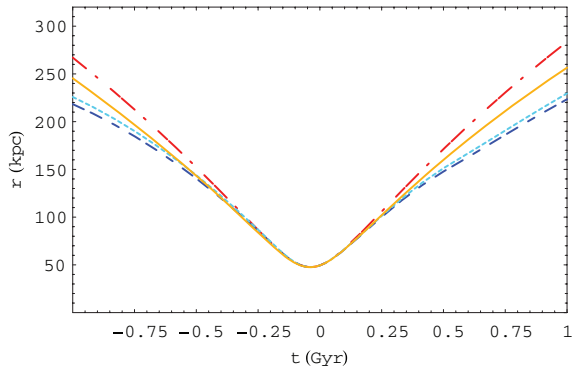
Figure 3. LMC: galactocentric distance r, in kpc, for $-1 \leq t \leq 1$ Gyr. Red dash–dotted line: CDM. Blue dashed line: MOND ($\mu = X/(1 + X)$). Light blue dotted line: MOND ($\mu = X$). Yellow continuous line: MOG. The initial condition is $r = 49.4$ kpc for the position; for the velocity, the central values of Table 1 have been adopted. No dynamical friction has been applied in CDM and MOND. For the mass of the SMC the total value (baryonic + dark matter) has been adopted for CDM, while that encompassing only baryonic components has been used for MOG and MOND. The time-span of the integration is $-1 \leq t \leq 1$ Gyr.

Fig. 3 shows the impact of the dynamical friction; after $+1$ Gyr, without modelling it in CDM and MOND, the mutual difference between CDM and MOG tends to increase by about 10 kpc, while the MONDian trajectories are left almost unaffected. Instead, at -1 Gyr the discrepancy between CDM and MOG gets reduced by 10 kpc, while the MOND distance is smaller by about 20 kpc.

The impact of the uncertainties in the velocity components of the LMC has been evaluated as will be done for the SMC in Section 2.2; it is shown in the upper (minimum velocity) and lower (maximum velocity) panels of Fig. 2. Differences with respect to the nominal case are present. Indeed, for the smallest value of the velocity ($\dot{x}_0 = -86 + 12 = -74$ km s^{-1}, $\dot{y}_0 = -268 + 11 = -257$ km s^{-1}, $\dot{z}_0 = 252 - 16 = 236$ km s^{-1}), the overall discrepancy between CDM/MOG and MOND is of the order of 50–60 kpc after $+1$ Gyr, with a reduction in the final distances in CDM/MOG with respect to the middle panel of Fig. 2 (20 kpc for CDM, 30 kpc for MOG and 50 kpc for MOND); -1 Gyr the CDM distance is 30 kpc smaller than for the nominal values of the velocity components, MOG is 35 kpc below the level of the middle panel of Fig. 2, while the MOND curves experience a reduction of about 40 kpc. For $\dot{x}_0 = -86 - 12 = -98$ km s^{-1}, $\dot{y}_0 = -268 - 11 = -279$ km s^{-1}, $\dot{z}_0 = 252 + 16 = 268$ km s^{-1}, corresponding to the maximum velocity, the relative discrepancy after $+1$ Gyr among the various models is about 60–80 kpc, with an increase in each of them with respect to the middle panel of Fig. 2 (25 kpc for CDM, 30 kpc for MOG, and 50–60 kpc for MOND); also at -1 Gyr there is an overall increase with respect to the case of the nominal values of the velocity components (20 kpc for CDM, 30 kpc for MOG and 30–40 kpc for MOND).

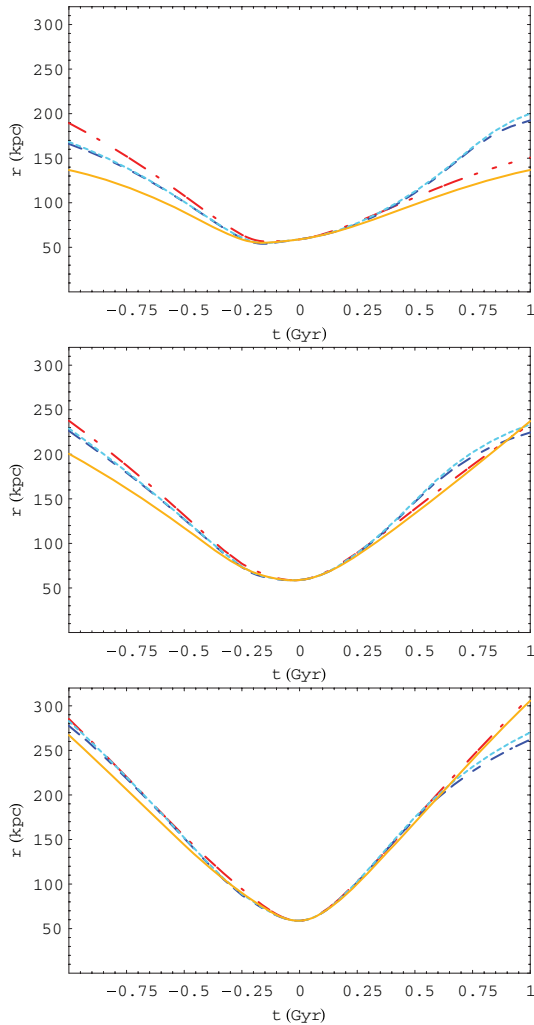## 2.2 The Small Magellanic Cloud

Fig. 4 depicts the sections in the coordinate planes of the SMC's orbits over $-1 \leq t \leq 1$ Gyr for CDM (red dash–dotted curves), MOND (blue dashed lines and light blue dotted lines) and MOG (yellow continuous curves) by using the central values of the initial velocities of Table 2 and the same values of Section 2.1 for the masses of MW and MCs and of the other model parameters. Concerning MOND and the impact of EFE, we followed the same approach as
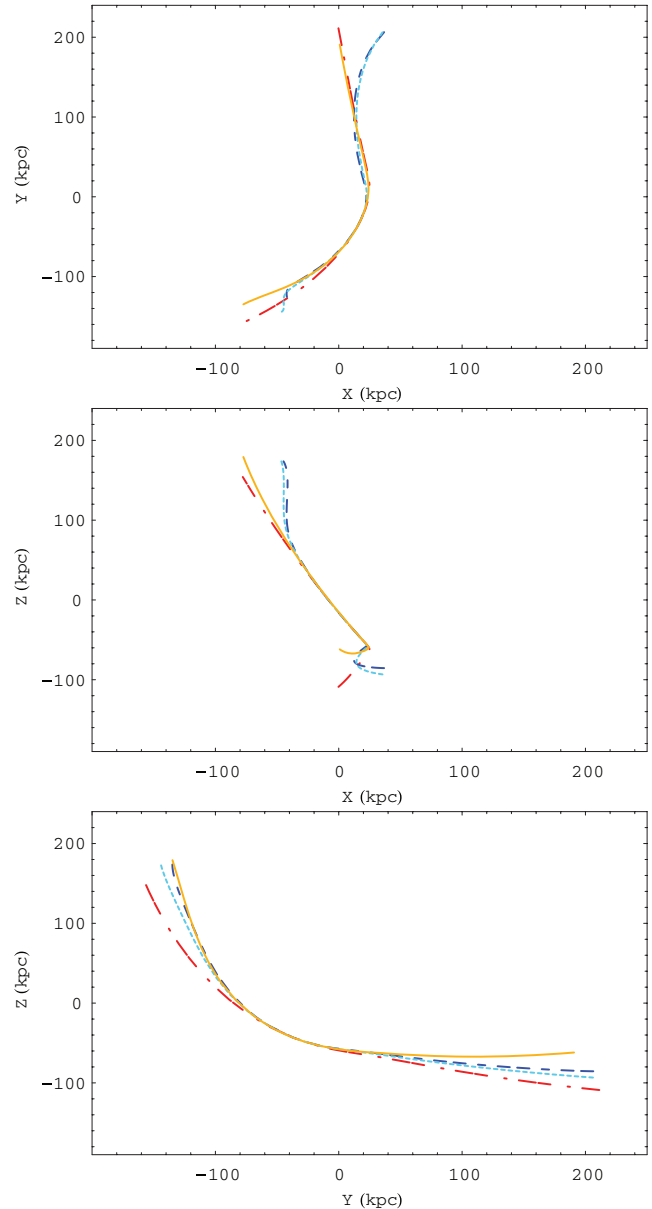
Figure 4. Sections in the coordinate planes of the numerically integrated trajectories of the SMC experiencing (a) the Newtonian acceleration with CDM (red dash–dotted line), (b) the MOND acceleration with $\mu = X/(1 + X)$ (blue dashed line), (c) the MOND acceleration with $\mu = X$ (light blue dotted line) and (d) the MOG acceleration (yellow continuous line). The central values of the initial conditions of Table 2 have been used. For the baryonic masses of the MW's bulge and disc we used the values by McGaugh (2008), with a total baryonic mass of $M = 6.5 \times 10^{10}$ M$_\odot$. For the masses of MCs, entering their mutual interactions and the dynamical friction, both modelled in this integration, the total values (baryonic + dark matter) have been adopted for CDM, while those encompassing only baryonic components have been used for MOG and MOND.. The time-span of the integration is $-1 \leq t \leq 1$ Gyr.

for the LMC in Section 2.1. It can be noted that MOND, MOG and CDM yield different orbital patterns, especially in the $\{xy\}$ and $\{xz\}$ planes, and it is possible, in principle, to discriminate among them.

In the middle panel of Fig. 5, we plot the time evolution of the Galactocentric distance of the SMC according to CDM, MOND and
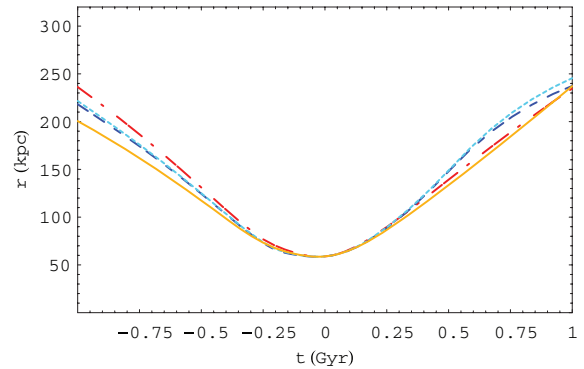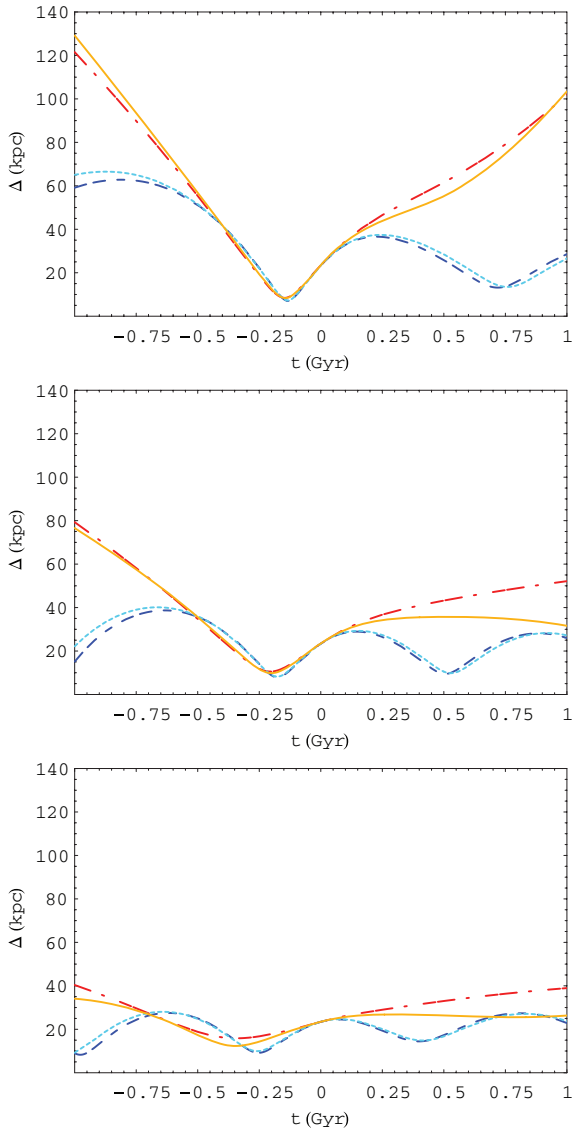
Galactocentric distance of the SMC for the maximum value of its speed, i.e. $v_{\rm SMC} = 369\,{\rm km\,s^{-1}}$ corresponding to $\dot{x}_0 = -87 - 48 = -135\,{\rm km\,s^{-1}}$, $\dot{y}_0 = -247 - 42 = -289\,{\rm km\,s^{-1}}$, $\dot{z}_0 = 149 + 37 = 186\,{\rm km\,s^{-1}}$, is shown in the lower panel of Fig. 5. By comparing it with the middle panel of Fig. 5, it can be noted that, after $+1$ Gyr, the Galactocentric distance increases, in particular in CDM and MOG; in fact, at -1 Gyr the increase is more uniform for all the models. In the upper panel of Fig. 5 we depict the case for $\dot{x}_0 = -87 + 48 = -39\,{\rm km\,s^{-1}}$, $\dot{y}_0 = -247 + 42 = -205\,{\rm km\,s^{-1}}$, $\dot{z}_0 = 149 - 37 = 112\,{\rm km\,s^{-1}}$ yielding the minimum value for the SMC's speed $v = 236\,{\rm km\,s^{-1}}$. In this case, CDM and MOG yield a smaller Galactocentric distance after $+1$ Gyr: indeed, it is as large as 140–150 kpc. Instead, after -1 Gyr the MOND curves lie in between the MOG/CDM ones, with an overall reduction of 50–60 kpc for all the models.

2.3 The mutual distance between the SMC and LMC

In the middle panel of Fig. 7, the mutual SMC−LMC distance $\Delta = \sqrt{(x_{\rm LMC} - x_{\rm SMC})^2 + (y_{\rm LMC} - y_{\rm SMC})^2 + (z_{\rm LMC} - z_{\rm SMC})^2}$ is shown for the central values of the velocity components of both MCs and with the same model and parameter values of Section 2. The pattern by CDM is quite different with respect to those by MOND and, to a lesser extent, MOG, both in the size of the distance reached and, especially, in the temporal signature. After $+1$ Gyr, MOND exhibits a bounce yielding the smallest maximum reciprocal separation, i.e. about 25 kpc, while for CDM, which yields an increasing signal, it is approximately 50 kpc. Instead, at -1 Gyr CDM and MOG reach 80 kpc, while MOND is around 20 kpc.

In Fig. 8 we show the mutual distance of MCs without dynamical friction. After $+1$ Gyr, the CDM maximum distance is 60 kpc, while the MOND curves tend to approach the MOG one at 30 kpc. After -1 Gyr, CDM reaches about 70 kpc; MOND is below the 20 kpc level.
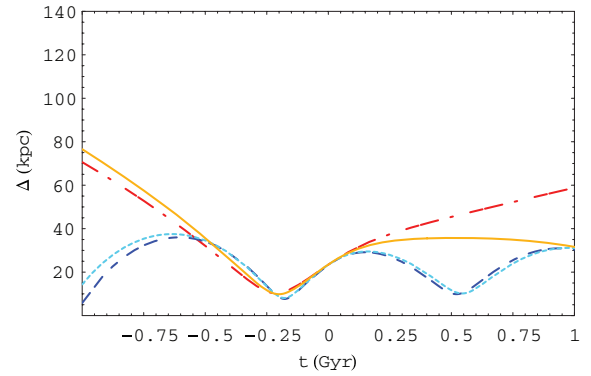
The impact of the uncertainties in the velocity of both SMC and LMC on the mutual separation is depicted in the upper and lower panels of Fig. 7, respectively. Low velocities (upper panel) yield a change in the bouncing time for MOND and an increase in Δ in CDM and MOG by more than 50 kpc for ± 1 Gyr. Also note

MOG in the next Gyr for the central values of the velocity components of Table 2. The distance reached in all the three models after $+1$ Gyr is practically the same, amounting to 220–230 kpc. After -1 Gyr the scatter among the models considered is larger, amounting to about 40 kpc. As for the LMC, all the models considered tend to undergo reciprocal departures after some about ± 500 Myr, although smaller.

Fig. 6 shows that switching off the dynamical friction in CDM and MOND does not substantially alter the overall picture.

The uncertainty in the velocity components of the SMC may have different consequences on its orbit for the models considered. The

Figure 8. Mutual distance Δ between the SMC and LMC, in kpc, for $-1 \leq t \leq 1$ Gyr. Red dash–dotted line: CDM. Blue dashed line: MOND [$\mu = X/(1 + X)$]. Light blue dotted line: MOND ($\mu = X$). Yellow continuous line: MOG. For the velocity components of both SMC and LMC, we used their central values. No dynamical friction has been modelled. For the masses of MCs, entering their mutual interaction, the total values (baryonic + dark matter) have been adopted for CDM, while those encompassing only baryonic components have been used for MOG and MOND.

3 SUMMARY AND CONCLUSIONS

We simultaneously integrated in a numerical way the orbits of both MCs for $-1 \leq t \leq 1$ Gyr within MOND, MOG and CDM to see if, at least in principle, it is possible to discriminate among them. This is, in principle, important also because it is believed that MS follows the orbits of MCs.

Since the LMC and SMC are at about 50–60 kpc from the GC, they are ideal candidates for investigating the deep MOND regime ($A_N/A_0 = 0.03$–0.02); moreover, the details of the realistic mass distribution can be neglected. Thus, for MOND (and MOG) we used a pointlike approximation for the baryonic mass of the MW; we tested it by successfully reproducing the orbital paths of the Sagittarius dwarf galaxy ($r = 17$ kpc) obtained by other researchers with the MONDian fully non-linear-modified Poisson equation. For CDM, we used a logarithmic halo potential which is able to reproduce the value of the Galactic mass at 60 kpc obtained independently by analysing different tracers. We also took into account the mutual interaction of MCs and, for MOND and CDM, the dynamical friction as well. For the masses of MCs, we used the total (baryonic + dark matter) values dynamically inferred in CDM and the smaller ones coming from the direct detection of the electromagnetic radiation emitted by stars and neutral gas in MOND and MOG.

It turns out that, in fact, CDM, MOND and MOG do yield different trajectories for the SMC and LMC. In general, the spatial extension of the sections of the orbits in the coordinate planes is larger for CDM and MOG with respect to MOND. The SMC experiences larger discrepancies among the various models than the LMC. Since for the MW $A_{ext} \approx 0.01 A_0$, we also investigated EFE in MOND by considering not only $A_{ext} \ll A_N$, $A_{ext} \ll A_0$, but also $A_{ext} \approx A_N$, $A_{ext} \ll A_0$ which cannot be excluded in view of the lingering uncertainty in MW's EFE. The resulting orbital patterns are rather similar to those obtained by neglecting A_{ext}. We also investigated the impact of the present-day uncertainties in the velocity components of MCs on their trajectories in the models considered by finding that it is more notable for the SMC than for the LMC; CDM and MOG are more sensitive to such a source of bias than MOND. In general, the largest discrepancies among the various models occur around ± 1 Gyr. This suggests that extending the

Figure 7. Mutual distance Δ between the SMC and LMC, in kpc, for $-1 \leq t \leq 1$ Gyr. Red dash–dotted line: CDM. Blue dashed line: MOND [$\mu = X/(1 + X)$]. Light blue dotted line: MOND ($\mu = X$). Yellow continuous line: MOG. Upper panel: for the velocity components of both SMC and LMC, we used their minimum values. Middle panel: for the velocity components of both SMC and LMC, we used their central values. Lower panel: for the velocity components of both SMC and LMC, we used their maximum values. For the masses of MCs, entering their mutual interactions and the dynamical friction, the total values (baryonic + dark matter) have been adopted for CDM, while those encompassing only baryonic components have been used for MOG and MOND.

the increase of the MOND curves at -1 Gyr: they pass from 20 to 60 kpc, while they are not substantially changed after $+1$ Gyr. On the contrary, high velocities (lower panel) tend to yield an overall reduction in the distances among all the models, with Δ_{CDM} reduced down to 40 kpc.

Generally speaking, the repeated close encounters (in MOND and MOG) may have an impact on the star formation history and/or morphology of both MCs; anyway, discussing such interesting issues is beyond the scope of this paper.

integration time may yield interesting findings; it may be the subject of further analyses. Over the time-scale considered, the dynamical friction does not make the paths too much different in the various models examined.

ACKNOWLEDGMENTS

REFERENCES

Angus G., McGaugh S., 2008, MNRAS, 383, 417
Begeman K., Broeils A., Sanders R., 1991, MNRAS, 249, 523
Bekenstein J., 2004, Phys. Rev. D, 70, 083509
Bekenstein J., 2006, Contemporary Phys., 47, 387
Bekenstein J., Magueijo J., 2006, Phys. Rev. D, 73, 103513
Bekenstein J., Milgrom M., 1984, ApJ, 286, 7
Bekki K., Chiba M., 2005, MNRAS, 356, 680
Besla G., Kallivayalil N., Hernquist L., Robertson B., Cox T. J., van der Marel R. P., Alcock C., 2007, ApJ, 668, 949
Binney J., Tremaine S., 1987, Galactic Dynamics. Princeton Univ. Press. Princeton, NJ, p. 747
Bosma A., 1981, AJ, 86, 1791
Brada R., Milgrom M., 1995, MNRAS, 276, 453
Bruneton J.-P., Esposito-Farèse G., 2007, Phys. Rev. D, 76, 124012
Cadoni M., 2004, Gen. Relativ. Gravit, 36, 2681
Capozziello S., Cardone V., Lambiase G., Troisi A., 2006, Int. J. Mod. Phys. D, 15, 69
Cioni M.-R., van der Marel R., Loup C., Habing H., 2000, A&A, 359, 601
Ciotti L., Binney J., 2004, MNRAS, 351, 285
Clewley L., Warren S., Hewett P., Wilkinson M., Evans N., 2004, in Ryder S., Pisano D., Walker M., Freeman K., eds, Proc. IAU Symp. 220, Dark Matter in Galaxies. Astron. Soc. Pac., San Francisco, p. 209
Connors T., Kawata D., Gibson B., 2006, MNRAS, 371, 108
Dopita M., Lawrence C., Ford H., Webster B., 1985, ApJ, 296, 390
Fabris J., Pereira Campos J., 2009, Gen. Relativ. Gravit., 41, 93
Famaey B., Binney J., 2005, MNRAS, 363, 603
Famaey B., Bruneton J.-Ph., Zhao H., 2007a, MNRAS, 377, L79
Famaey B., Gentile G., Bruneton J.-P., Zhao H., 2007b, Phys. Rev. D, 75, 063002
Frigerio-Martins C., Salucci P., 2007, MNRAS, 381, 1103
Gardiner L., Noguchi M., 1996, MNRAS, 278, 191
Gondolo P., 2004, Lectures Delivered at the NATO Advanced Study Institute Frontiers of the Universe, 2003 September 8–20, Cargese, France
Grillmair C., Dionatos O., 2006, ApJ, 643, L17
Haghi H., Rahvar S., Hasani-Zonooz A., 2006, ApJ, 652, 354
Haghi H., Hasani-Zonooz A., Rahvar S., 2009, New Astron., 14, 692
Hardy E., Suntzeff N., Azzopardi M., 1989, ApJ, 344, 210
Harris J., Zaritsky D., 2006, AJ, 131, 2514
Iorio L., 2008a, J. Gravit. Phys., 2, 26
Iorio L., 2008b, Schol. Res. Exchange, 2008, 238385
Iorio L., 2009, Ap&SS, 323, 215
Johnston K., Majewski S., Siegel M., Reid I., Kunkel W., 1999, AJ, 118, 1719
Kallivayalil N., van der Marel R., Alcock C., 2006, ApJ, 652, 1213

Khalil S., Muñoz S., 2002, Contemporary Phys., 43, 51
Kim S., Staveley-Smith L., Dopita M. A., Freeman K. C., Sault R. J., Kesteven M. J., McConnell D., 1998, ApJ, 503, 674
Knebe A., Gibson B., 2004, MNRAS, 347, 1055
Law D., Johnston K., Majewski S., 2005, ApJ, 619, 807
Llinares C., Knebe A., Zhao H., 2008, MNRAS, 391, 1778
McGaugh S., 2008, ApJ, 683, 137
Malekjani M., Rahvar S., Haghi H., 2009, ApJ, 694, 1220
Milgrom M., 1983a, ApJ, 270, 365
Milgrom M., 1983b, ApJ, 270, 371
Milgrom M., 1983c, ApJ, 270, 384
Milgrom M., 2008, Talk presented at the XIX Rencontres de Blois. http://arxiv.org/abs/0801.3133v2
Milgrom M., 2009, MNRAS, 399, 474
Miyamoto M., Nagai R., 1975, PASJ, 27, 533
Moffat J., Toth V., 2008, ApJ, 680, 1158
Moffat J., Toth V., 2009, Class. Quantum Gravity, 26, 085002
Nipoti C., Londrillo P., Zhao H., Ciotti L., 2007, MNRAS, 379, 597
Nipoti C., Ciotti L., Binney J., Londrillo P., 2008, MNRAS, 386, 2194
Persic M., Salucci P., Stel F., 1996a, MNRAS, 281, 27
Persic M., Salucci P., Stel F., 1996b, MNRAS, 283, 1102
Plummer H. C., 1911, MNRAS, 71, 460
Read J., Moore B., 2005, MNRAS, 361, 971
Rubin V., 1983, Sci, 220, 1339
Rubin V., Ford W., Thonnard N., Burstein D., 1982, ApJ, 261, 439
Salucci P., Borriello A., 2003, in Trampeti J., Wess J., eds, Lect. Notes in Phys. Vol. 616, Particle Physics in the New Millennium. Springer, Berlin, p. 66
Sánchez-Salcedo F., Reyes-Iturbide J., Hernandez X., 2006, MNRAS, 370, 1829
Sanders R., 2006, MNRAS, 370, 1519
Sanders R., McGaugh S., 2002, ARA&A, 40, 263
Sanders R., Noordermeer E., 2007, MNRAS, 379, 702
Schommer R., Suntzeff N., Olszewski E., Harris H., 1992, AJ, 103, 447
Sereno M., Jetzer Ph., 2006, MNRAS, 371, 626
Smith M. et al., 2007, MNRAS, 379, 755
Talmadge C., Berthias J.-P., Hellings R. W., Standish E. M., 1988, Phys. Rev. Lett., 61, 1159
Tiret F., Combes O., 2007, A&A, 464, 517
Tiret F., Combes O., 2008, A&A, 483, 719
van der Marel R., Alves D., Hardy E., Suntzeff N., 2002, AJ, 124, 2639
van der Marel R., Kallivayalil N., Besla G., 2009, in van Loon J. Th., Oliveira J. M., eds, Proc. IAU Symp. 256, The Magellanic System: Stars, Gas, and Galaxies. Cambridge Univ. Press, Cambridge, p. 89
Willett B., Newberg H., Zhang H., Yanny B., Beers T., 2009, ApJ, 697, 207
Wu X., Zhao H., Famaey B., Gentile G., Tiret O., Combes F., Angus G. W., Robin A. C., 2007, ApJ, 665, L101
Wu X., Famaey B., Gentile G., Perets H., Zhao H., 2008, MNRAS, 386, 4, 2199
Xue X.-X. et al., 2008, ApJ, 684, 1143
Yoshizawa A., Noguchi M., 2003, MNRAS, 339, 1135
Zhao H., 2007, ApJ, 671, 1, L1
Zhao H., Famaey B., 2006, ApJ, 638, L9
Zwicky F., 1933, Helvetica Phys. Acta, 6, 110

This paper has been typeset from a TEX/LATEX file prepared by the author.